

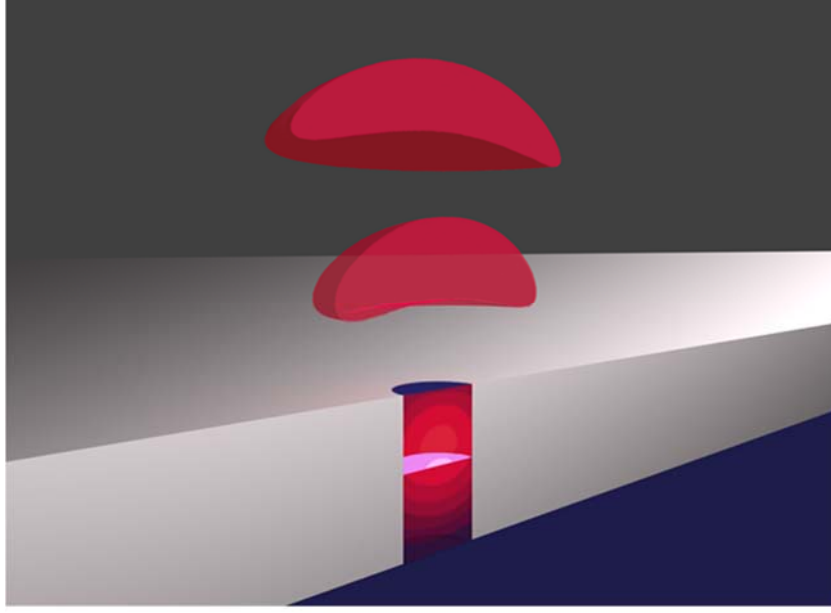
A Light-Matter Interface based on a Single InAs/GaAs Quantum Dot in a Nanometallic Cavity

Yousif A. Kelaita^{*,1}, Kevin A. Fischer^{*,1}, Thomas M. Babinec¹, Konstantinos G. Lagoudakis¹, Tomas Sarmiento¹, Armand Rundquist¹, Arka Majumdar^{1,2}, Jelena Vučković¹

1. Department of Electrical Engineering and Ginzton Laboratory, Stanford University, Stanford, CA 94305, USA.
2. Department of Electrical Engineering and Department of Physics, University of Washington, Seattle, WA-98195, USA.

Abstract

Despite tremendous advances in the fundamentals and applications of cavity quantum electrodynamics with single InAs/GaAs quantum dots, investigations in this field have been limited to optical cavities composed of purely dielectric materials^{1,2}. Here, we demonstrate for the first time the coupling of an InAs/GaAs quantum dot to a hybrid metal/semiconductor nanocavity consisting of a GaAs nanocylinder embedded in a metallic film. Key features of our nanometallic light-matter interface include: (i) order of magnitude reduction in mode volume compared to that of leading photonic crystal CQED systems, resulting in a maximum atom-field coupling rate of $g/(2\pi) \sim 180$ GHz for InAs/GaAs quantum dots; (ii) surface-emitting nanocylinder geometry and therefore good collection efficiency compared to the bulk ($\sim 5X$ enhancement); and finally (iii) strong and broadband spontaneous emission rate enhancement (Purcell factor ~ 8). This light-matter interface may play an important role in the fundamentals of cavity quantum electrodynamics³ as well as in its application to optical interconnects⁴ and quantum networks⁵⁻⁷.



A prototypical cavity quantum electrodynamics (CQED) system that consists of a quantum emitter in an optical cavity is characterized by three rates (γ , κ , g), including the emitter decay rate γ , cavity field decay rate κ , and coherent emitter-cavity coupling rate g ⁸. The coherent coupling rate scales as $g \propto 1/\sqrt{V}$, where V is the cavity mode volume, and increasing field localization has therefore long been recognized as a path to boosting emitter-field coupling strength⁹⁻¹³. For example, whispering gallery GaAs microdisk resonators exhibit mode volumes $V \sim 5 (\lambda/n)^3$ and coupling to InAs quantum dots with rate $g/(2\pi) \sim 2 - 3$ GHz¹. Planar photonic crystal nanocavities possess an order of magnitude smaller mode volume $V \sim 0.5 (\lambda/n)^3$ with light-matter coupling strengths up to $g/(2\pi) \sim 40$ GHz^{2,14,15}. Moving beyond this nanophotonic CQED regime and achieving $g/(2\pi) > 40$ GHz requires coupling a single quantum emitter to a nanoscale cavity characterized by deep sub-wavelength optical confinement^{16,17}. However, there have been no related reports with InAs/GaAs quantum dots (QDs), which are the only solid-state quantum emitters for which the strong coupling regime of CQED has been reached^{14,18}.

The hybrid metal/semiconductor CQED system investigated in this Letter (Fig. 1) is a variation on recent theoretical proposals^{10,19} and an integrated solid-state alternative to early demonstrations with other emitters such as dye molecules and

colloidal quantum dots²⁰⁻²⁴. Our quantum emitter consists of the excitation of a bound electron-hole pair (neutral exciton X^0) confined in a self-assembled InAs quantum dot grown by the Stranski-Krastanov process. Individual InAs quantum dots are roughly ~ 20 nm in cross section with the active layer located ~ 100 nm below the top surface of the GaAs wafer. The InAs quantum dot is contained within a GaAs nanopillar of radius $r \sim 40 - 50$ nm and height $h \sim 200$ nm (Fig. 1a), which is itself embedded inside of a silver film (Fig. 1b). This GaAs nanopillar supports degenerate \hat{x} and \hat{y} polarized TE_{11} waveguide modes with the silver film generating optical confinement in the cylinder cross-section (Fig. 1c). Impedance mismatch between the waveguide, GaAs substrate and free-space indices generates optical confinement vertically along the nanocylinder, with a local field intensity of $E/E_{Max} \sim 0.8$ approximately overlapping the quantum dot layer (Fig. 1d). InAs quantum dots positioned within ~ 20 nm of surfaces are well-known to have quenched and broadened emission²⁵, and thus only quantum dots located near the nanocylinder center may be optically active and exhibit narrow lines. In Fig. 1d, the dashed line indicates the disk in which QDs must be located to avoid such nonradiative quenching.

An exciton confined to the InAs quantum dot and embedded within the nanometallic cavity may decay via emission of a photon polarized into either of the orthogonal TE_{11} nanocylinder modes. Moreover, the spontaneous emission rate is enhanced from the bulk rate due to the enhanced density of optical states (Purcell effect). Finite-difference time-domain simulations show that the nanocylinder cavities possess resonances with quality factor $Q \sim 25$ and ultra-small mode volumes $V \sim 0.025 * (\lambda/n)^3$ at the emission wavelength, with maximum achievable Purcell factor $F_P = \tau_{Bulk} / \tau_{Cavity} \sim 30 - 40$. In this case, application of the dipole approximation is valid despite the small size of the cavity since the gradient of the field at the QD position is negligible²⁶. Simultaneously, the overall photon collection efficiency is also improved due to an antenna effect. With the numerical aperture $NA \sim 0.75$ lens used in our experimental setup, only $\eta_{col} \sim 1.5\%$ of the photons emitted by a QD dipole embedded in a bulk (unprocessed) sample may be collected due to total internal reflection at the air-GaAs interface. On the other hand, FDTD simulations indicate that

the lens collects $\eta_{\text{col}} \sim 7\%$ of the photons coupled to the nanocylinder cavity mode shown in Fig. 1. Further fabrication and simulation details can be found in the Methods and Supporting Information sections.

Roughly one in ten fabricated cavities exhibited multiple emission lines from a variety of QD states, including the neutral exciton (X^0), charged exciton (X^- , X^+) and bi-exciton (XX). Using a linear polarizer, we may select the orthogonal \hat{x} and \hat{y} cavity directions and indeed these show an identical photoluminescence spectrum of emission lines with nearly equal intensity (Fig. 2a, black and blue data). Moreover, the intensity of these quantum dots is quite bright with approximately $\sim 8 - 10 \times$ improvement compared to individual lines addressed in a bare nanopillar (Fig. 2a, green data) and $\sim 50 \times$ compared to unprocessed bulk material (data not shown). The bare nanopillar is $\sim 4 - 5 \times$ brighter than bulk material due to the increased photon collection efficiency resulting from geometric effects, and hence the further enhancement provided by the nanometallic cavity is subsequently evaluated as a Purcell effect. In some of the nanometallic cavity devices (not used for the presented experiments), significant broadening of all transitions suggests that the quantum dots were located in close proximity to the GaAs/Ag interface. Measurement of the intensity autocorrelation function $g^{(2)}(\tau) = \langle I(t) I(t + \tau) \rangle / \langle I(t) \rangle^2$ of the neutral exciton line X^0 for quasi-resonant excitation in a Hanbury Brown and Twiss (HBT) experiment shows strong anti-bunching $g^2_{(X,Y)}(0) \sim (0.12, 0.19)$, confirming the presence of a single quantum emitter coupled to both orthogonal cavity modes (Fig. 2c, 2d).

After demonstrating that we may optically address a single exciton line in the cavity, we now characterize its properties as a single photon source. To do so, we measure the number of single photon counts detected per second (CPS) as a function of incident optical pump power (P , measured before the objective lens) under quasi-resonant, pulsed excitation (Fig. 2b). We perform pulsed excitation with 80MHz repetition rate. As is expected for a two-level system, we observe that the number of single photon counts increases linearly at low pump power and saturates at high powers²⁷. Considering that we utilize pulsed excitation with repetition period much

longer than the excitonic lifetime, the saturation power is not dependent on the modified excitonic lifetime. However, the single photon counts in saturation are large thanks to strong Purcell enhancement and hence an increase in the spontaneous emission coupling factor β , in addition to an improvement in collection efficiency coming from the structure geometry.

Measurements of the far-field emission profile from the structure are shown in Fig. 3. Here, quasi-resonant excitation of the quantum dot X^0 line was imaged onto a low-noise CCD using a single lens to generate the Fourier transform of the spatial emission profile (k-space image). We observe a nearly circularly symmetric, Gaussian far-field pattern for a single X line in both \hat{x} and \hat{y} orientations.

We conclude with a characterization of the optical properties of single photons generated by the nanocylinder cavity. First, we establish the roughly unmodified spontaneous emission decay $\tau_{Bulk} = 1.02 \pm 0.033$ ns via pulsed excitation of an exciton in a nanopillar device ($r \sim 200$ nm) and imaging on a streak camera (Fig. 4a). Next, we performed the same measurement for the exciton coupled to both orthogonal modes of our nanometallic cavity. We observe modified QD lifetimes of $\tau_X = 142 \pm 7$ ps and $\tau_Y = 156 \pm 4$ ps (Fig. 4b-c). Small deviations in QD lifetimes for orthogonal polarizations may arise either from ellipticity in the pillars or positioning of the QD off of the center of the nanopillar axis. Justified by the large single photon counts observed from this device, we attribute the full intensity decay rate modification to the Purcell effect and estimate Purcell factor $F_{P,X,Y} \sim 7 - 8$ for a single quantum dot. Because the metallic losses only affect the damping of the cavity mode (and not of the emitter itself, based on the unmodified emitter linewidth in a nanometallic cavity), the calculation of the Purcell factor can be performed in the same way as for a lossy dielectric cavity. Such a Purcell factor would already redirect nearly all of the QD spontaneous emission into the nanocavity mode, with the spontaneous emission coupling factor $\beta \approx \frac{F_p}{F_p + 1}$ being near unity. We note that such

a bimodal cavity-enhanced spontaneous emission rate has traditionally been more challenging to implement in photonic crystals due to higher sensitivity to fabrication

imperfections²⁸. Finally, to justify that the emitter itself is not significantly nonradiatively affected by the proximity of the metal, we measure the coherence time of this QD exciton with a Michelson interferometer (Fig. 4d) and obtain $\tau_c = 77 \pm 2$ ps. Therefore, the coherence time is close to the lifetime measured from the intensity decay, indicating that the linewidth is primarily radiatively limited, and that the 8-fold reduction in the intensity decay of the QD in the nanometallic cavity has to result from radiative effects.

In conclusion, we have demonstrated a novel and versatile light-matter interface for single InAs/GaAs quantum dots in semiconductor CQED. Key features of our platform include very small mode volume, a surface emitting nanocylinder geometry, and strong and broadband spontaneous emission rate modification via metallic confinement. In the future, further engineering of the system (such as the use of site-controlled QDs) should allow for improved properties. Furthermore, electrical injection and QD charge state control are possible in this system, in addition to broadband bimodal enhancement as is critical for quantum information technologies²⁸. Finally, this light-matter interface can also be implemented in emerging room-temperature quantum systems such as in diamond²⁹ and silicon carbide³⁰.

Methods

Device Design. Finite-difference time-domain calculations were performed using the commercial package Lumerical to obtain resonance spectra, mode profiles, and far-field profiles. The simulations presented in the text were performed for a device with a radius of 50 nm and height of 200 nm using permittivity values for GaAs at low temperatures ($n = 3.5$) and Palik data for silver³¹. Resonances were excited using a broadband Gaussian pulse incident from above the cavity, and the spectrum was obtained with a Fourier transform of the time-dependent electric field inside the cavity. Mode profiles were obtained by calculating a running Fourier transform and post-selecting the Fourier component corresponding to the cavity resonance. The far-field emission pattern is generated by projecting fields at a plane located 50 nm above

the device. Mode volumes were calculated according to $V = \iiint \frac{\partial(\omega\epsilon(r))}{\partial\omega} * |\vec{E}(\vec{r})|^2 dV / \max[\frac{\partial(\omega\epsilon(r))}{\partial\omega} * |\vec{E}(\vec{r})|^2]$ ³². However, we emphasize that factors such as nanometer-scale imprecision in the GaAs nanopillar radius, slight ~ 5 - 10° tapering in the GaAs nanopillar sidewalls, minor imperfections in the silver film deposition, and approximate values in metal permittivity can result in significant modifications to the resonant wavelength, mode profile, and cavity Q and V in our calculations. The device's far-field profile, however, was mostly insensitive to any of the aforementioned changes. This nominal device design therefore provided a general guideline for the devices investigated in experiment. From the expression for the maximum coupling strength $g^2 = \mu^2\omega/(\hbar\epsilon_0 n^2 V)$ and the bulk spontaneous emission rate $\Gamma_{bulk} = 8\pi^2 n \mu^2 / (3\epsilon_0 \hbar \lambda^3)$ of an InAs QD with dipole moment μ in GaAs with refractive index $n = 3.5$, we can extract the maximum achievable value of $g/(2\pi) = 180\text{GHz}$ in this nanometallic cavity.

Device Fabrication. The cavities demonstrated in this experiment were fabricated on a sample containing a single layer of self-assembled Stranski-Krastanov InAs quantum dots grown by molecular beam epitaxy on a GaAs substrate and capped by a 100 nm GaAs layer. The quantum dot density is $60 - 80 / \mu\text{m}^2$ for the InAs/GaAs material used in this study, which corresponded to a density of ~ 1 quantum dot per device. In order to generate a mask for the nanopillar structures we first spun a solution of positive-tone ZEP 520A resist at a thickness of 300 nm, and patterned arrays of annuli with fixed $2.5 \mu\text{m}$ outer radius and variable 50 - 80 nm inner radius using a JEOL electron-beam lithography system at a base dose of $250 \mu\text{C}/\text{cm}^2$. After development of the exposed annuli, the remaining inner circular disk served as an etch mask for generating cylindrical nanopillars in GaAs via etching in an Oxford PlasmaPro inductively coupled plasma reactive ion etching system. A BCl_3 and Ar chemistry allowed us to generate a near vertical etch profile at a height of approximately 200 nm. Next, a 5 nm Cr adhesion layer followed by a 200 nm thick Ag film was deposited using electron-beam evaporation. Finally, soaking in acetone, IPA,

and n-Methyl-2-pyrrolidone (NMP) lifted off the remaining ZEP 520A and overlying Ag film.

Optical Characterization. Neutral quantum dot experiments were performed in a He-flow cryostat at low temperature (4K), necessary to preserve quantum confinement inside the InAs/GaAs QDs. We have employed micro-photoluminescence spectroscopy setup, similar to the one used in our earlier work¹⁴. Quantum dots in the cavities were first characterized using above band CW excitation with a 780 nm diode laser, followed by characterization under quasi-resonant excitation with ~ 3 ps pulses from a Ti:Sapphire laser (Newport-Spectra Physics Tsunami). Quantum dot emission was collected through a Zeiss objective lens with NA ~ 0.75 and optionally filtered using two Semrock narrow-bandpass filters (~ 2 nm). Observation of excitation polarization memory for quasi-resonant drive required polarizing the excitation path. Photoluminescence spectra and coherence length measurements were taken using a 0.75 m long Princeton Instruments Acton Pro spectrometer. Our device's X transition showed a narrow optical linewidth, confirmed with first order autocorrelation measurements. Similar coherence times were observed among the bulk dots surveyed on our sample. Perkin Elmer avalanche photodiodes (APD) detected single photon events with an efficiency of $\sim 40\%$ for second order autocorrelation and intensity saturation measurements. Bulk QD intensity decay occurred on long enough time scales to be measured with these APDs while intensity decay from the metal nanostructures occurred faster than the APD time resolution limit. Thus, measurement of this intensity decay required the use of a Streak camera (Hamamatsu). Our PL imaging setup has an estimated overall transmission efficiency of $\sim 22\%$. Finally, the far-field emission was imaged using a low-noise DVC CCD camera.

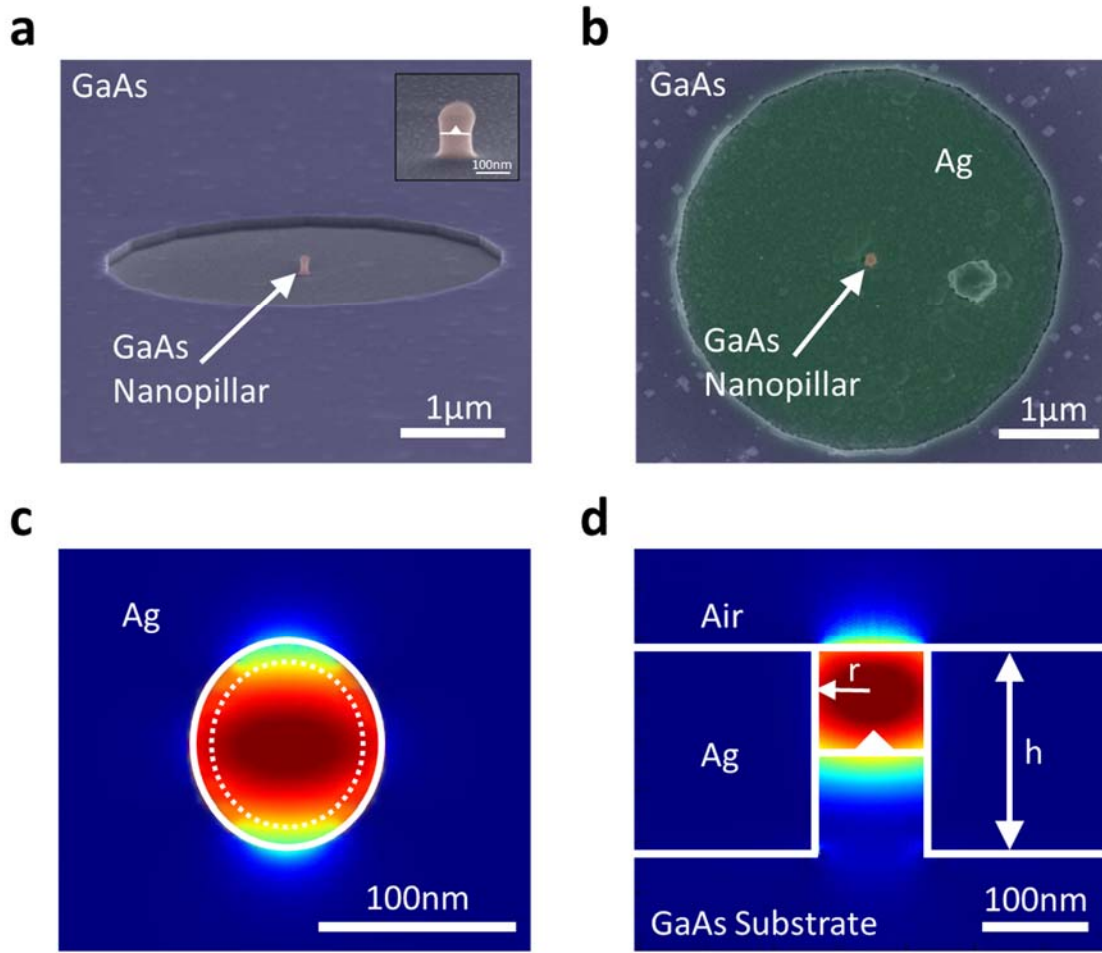


Figure 1. A nanometallic light-matter interface for a single InAs/GaAs quantum dot. **(a)** False-color SEM micrograph of the side profile of a bare GaAs nanopillar structure before metal deposition and lift-off. A slight undercut profile can be observed. The position of the InAs quantum dot layer is also indicated in the inset. **(b)** False-color SEM micrograph of the final nanocylinder cavity taken top-down. **(c, d)** FDTD simulation of the nanocylinder cavity field intensity ($|E_x|^2$) for one of two degenerate TE_{11} waveguide modes viewed in the nanocylinder cross-section (c) and along the nanocylinder axis (d). Due to surface effects, the quantum dot must be located within the dashed circle (c).

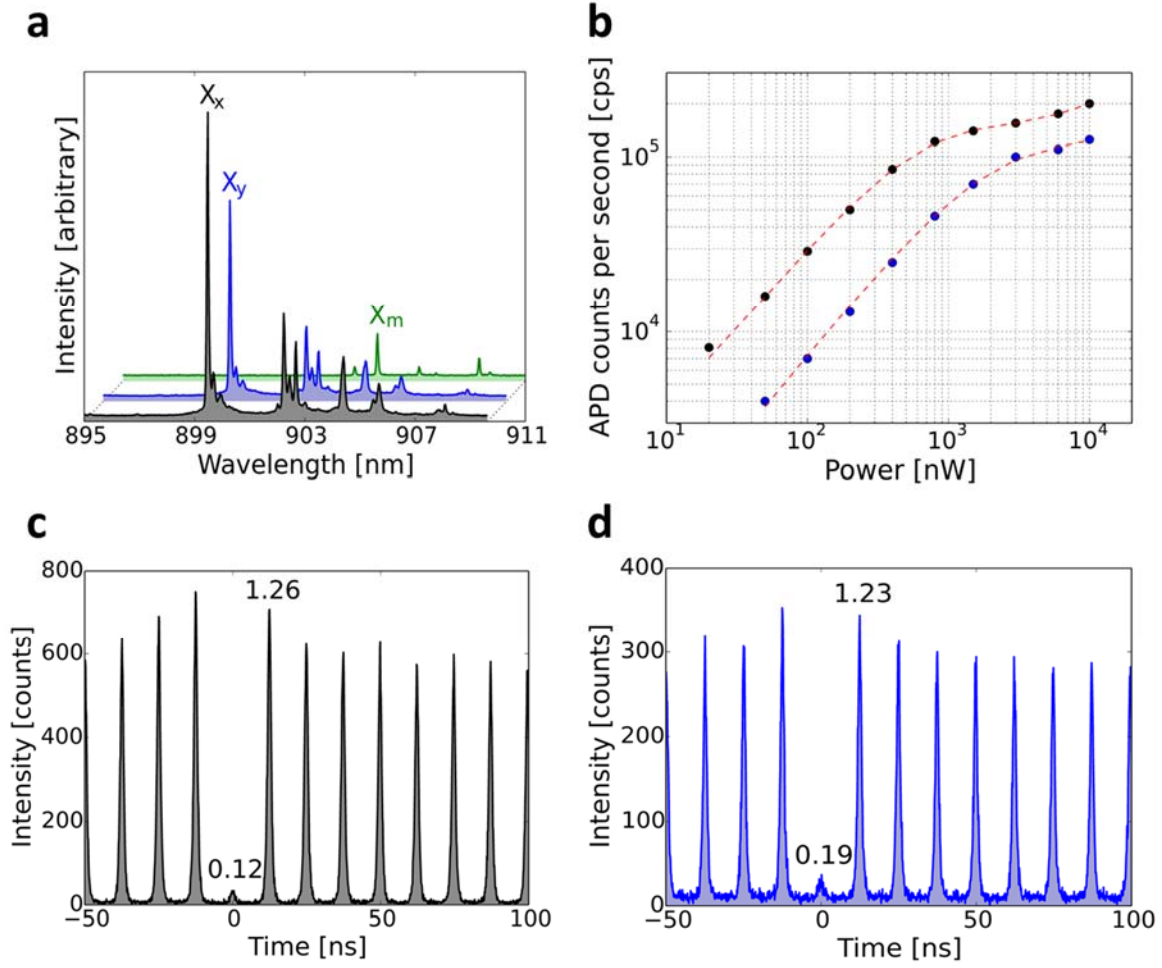


Figure 2. Demonstration of bimodal coupling between a single InAs/GaAs quantum dot and the nanometallic cavity. **(a)** Representative photoluminescence spectrum of a nanocavity containing a single quantum dot shows many emission lines due to different QD excitonic configurations (e.g. neutral-, charged-, and bi-exciton). The single exciton (X) line is highlighted for coupling to two orthogonal nanometallic cavity polarizations X_x (black) and X_y (blue) and a reference bare mesa X_m (green) that are offset horizontally and vertically for clarity. **(b)** Total number of single photons collected per second (circles) for quasi-resonant excitation of the exciton lines X_x and X_y . The horizontal axis corresponds to incident power, measured before the objective lens, and the source is excited with pulses at an 80MHz repetition rate. Fitting photon counts data to a saturation model incorporating linear background gives $\text{CPS}_{\text{Sat}} = (1.35 \cdot 10^5, 1.01 \cdot 10^5)$ [cps] and $\text{PSat} = (430, 1280)$ [nW] for (\hat{x}, \hat{y}) cavity polarizations. **(c, d)** Intensity autocorrelation $g^{(2)}(\tau)$ measurements for the exciton

line well above saturation powers show strong photon anti-bunching $g^{(2)}(0) \sim 0.12$ for \hat{x} (c) and $g^{(2)}(0) \sim 0.19$ for \hat{y} (d) polarizations. The autocorrelation measurements are normalized to integrated peak values at large times ($\tau \gg 0$).

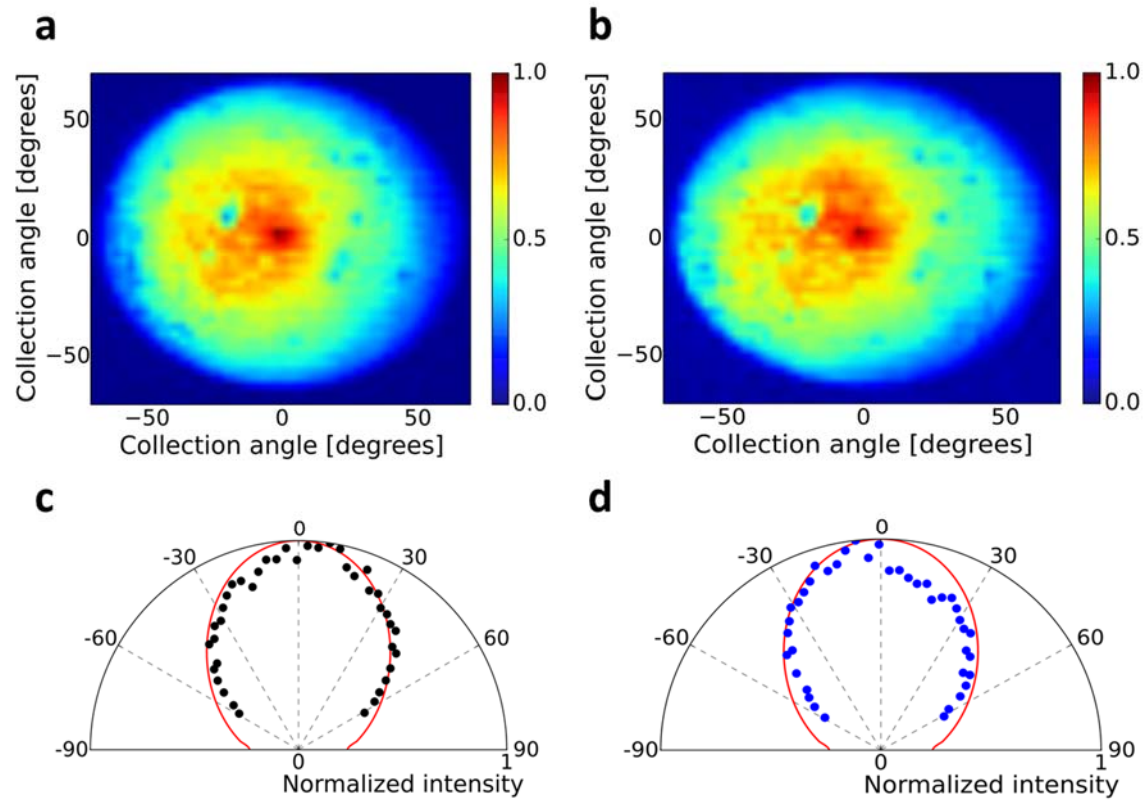


Figure 3. Observation of a far-field emission pattern from the neutral exciton line of a single InAs/GaAs quantum dot in the nanocavity. (a, b) Fourier space image for the X_x and X_y exciton lines. (c, d) Polar graph of $k_y = 0$ profiles of (a) and (b) show good agreement with far-field profiles obtained via FDTD (red lines).

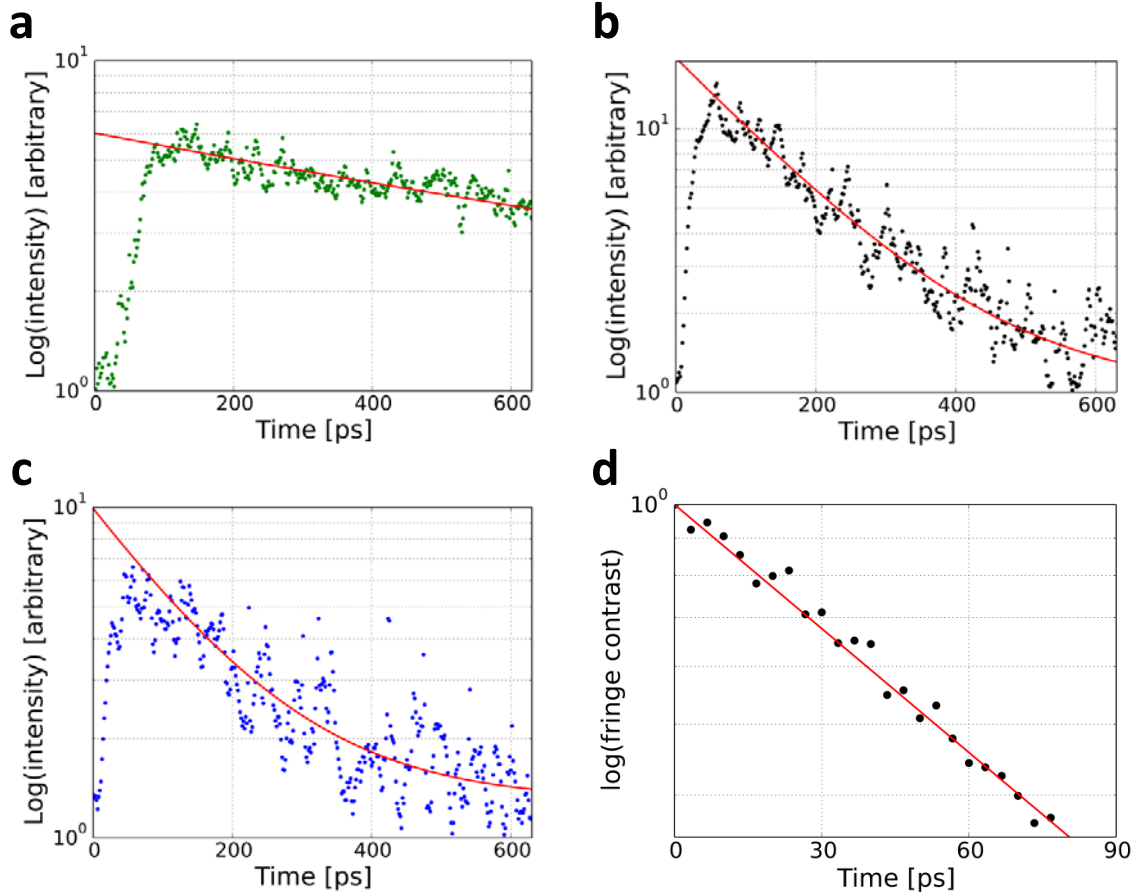


Figure 4. Emission properties for a single InAs/GaAs quantum dot in the nanometallic cavity. Fluorescence decay measurements taken with a streak camera show **(a)** $\tau = 1.02 \pm 0.033$ ns for an exciton line in a bare mesa, **(b)** $\tau_X = 142 \pm 7$ ps for the exciton line X_X in a nanometallic cavity, and **(c)** $\tau_Y = 156 \pm 4$ ps for the exciton line X_Y in a nanometallic cavity. **(d)** Coherence time measurement of the excitonic line in the nanometallic cavity performed using a Michelson interferometer, showing contrast as a function of path-length difference, yields $\tau_c = 77 \pm 2$ ps. Red curves provides a mono-exponential fit to the data in (a-d).

Author Information.

Corresponding Authors:

*Email: ykelaita@stanford.edu

Author Contributions:

* Y.A.K, and K.A.F. contributed equally to the contents of this manuscript.

Acknowledgements.

Y.A.K. acknowledges support from the Department of Defense (DoD) through the National Defense Science & Engineering Graduate Fellowship (NDSEG) Program and from the Stanford Graduate Fellowship (SGF). K.A.F. acknowledge support through Lu Stanford Graduate Fellowship. T.M.B. acknowledges support through the Nanoscale and Quantum Science and Engineering Postdoctoral Fellowship at Stanford. K.G.L. acknowledges support from the Swiss National Science Foundation. We are grateful to Prof. Jim Harris (Stanford University) for use of his MBE facilities. Also, we acknowledge Rich Tiberio with the Stanford Nano Center (SNC) for assistance in fabricating samples and Irena Fischer-Hwang for assistance with SEM figure preparation. This work is supported by the U.S. Air Force of Scientific Research Multidisciplinary University Research Initiative (AFOSR-MURI) on Quantum Metaphotonics and Metamaterials grant no. FA-9550-12-1-0488, and in part by the US Air Force Office of Scientific Research, MURI Center for Multifunctional Light-Matter Interfaces Based on Atoms and Solids.

References

- 1 Srinivasan, K.; Painter, O. Linear and nonlinear optical spectroscopy of a strongly coupled microdisk-quantum dot system. *Nature* **2007**, 450, 7171.
- 2 Englund, D.; Fattal, D.; Waks, E.; Solomon, G.; Zhang, B.; Nakaoka, T.; Arakawa, Y.; Yamamoto Y.; Vučković, J. Controlling the spontaneous emission rate of single quantum dots in a two-dimensional photonic crystal. *Phys. Rev. Lett.* **2005**, 95, 013904.
- 3 Haroche, S. Nobel Lecture: Controlling photons in a box and exploring the quantum to classical boundary. *Rev. Mod. Phys.* **2013**, 85, 1083-1102.
- 4 Miller, D. A. B. Device requirements for optical interconnects to silicon chips. *Proceedings of the IEEE* **2009**, 97, 1166-1185.
- 5 Kimble, H. J. The quantum internet. *Nature* **2008**, 453, 1023-1030.
- 6 Greve, K. d.; Yu, L.; McMahon, P. L.; Pelc, J. S.; Natarajan, C. M.; Kim, N. Y.; Abe, E.; Maier, S.; Schneider, C.; Kamp, M.; Hoefling, S.; Hadfield, R. H.; Forchel, A.; Fejer M. M.; Yamamoto, Y. Quantum-dot spin-photon entanglement via frequency downconversion to telecom wavelength. *Nature* **2012**, 491, 421-425.
- 7 Gao, W. B.; Fallahi, P.; Togan, E.; Miguel-Sanchez, J.; Imamoglu, A. Observation of entanglement between a quantum dot spin and a single photon. *Nature* **2012**, 491, 426-430.
- 8 Kimble, H. J. In *Cavity quantum electrodynamics*; Academic Press: Boston, 1994; Ch. 7.
- 9 Schuller, J. A.; Barnard, E. S.; Cai, W.; Jun, Y. C.; White, J. S.; Brongersma, M. L. Plasmonics for extreme light concentration and manipulation. *Nat. Mat.* **2010**, 9, 193-204.
- 10 Maksymov, I. S.; Besbes, M.; Hugonin, J. P.; Yang, J.; Beveratos, A.; Sagnes, I.; Robert-Philip, I.; Lalanne, P. Metal-coated nanocylinder cavity for broadband nonclassical light emission. *Phys. Rev. Lett.* **2010**, 105, 180502.
- 11 Engheta, N. An idea for thin subwavelength cavity resonators using metamaterials with negative permittivity and permeability. *IEEE Antennas and Wireless Propagation Letters* **2002**, 1, 10-13.

- 12 *MURI for Quantum Metaphotonics and Metamaterials*, <
http://quantummetaphotonics.com >
- 13 Vahala, K. J. Optical microcavities. *Nature* **2003**, 424, 839-846.
- 14 Englund, D.; Fararon, A.; Fushman, I.; Stolz, N.; Petroff, P.; Vuckovic, J. Controlling cavity reflectivity with a single quantum dot. *Nature* **2007**, 450, 857-861.
- 15 Takamiya, D.; Ota, Y.; Ohta, R.; Takagi, H.; Kumagai, N.; Ishida, S.; Iwamoto, S.; Arakawa, Y. in *2013 Conference on Lasers and Electro-Optics Pacific Rim (CLEO-PR), MI2-2 (2013)*.
- 16 Kühn, S.; Håkanson, U.; Rogobete, L.; Sandoghdar, V. Enhancement of single-molecule fluorescence using a gold nanoparticle as an optical nanoantenna. *Phys. Rev. Lett.* **2006**, 97, 017402.
- 17 Choy, J. T.; Hausmann, B. J. M.; Babinec, T. M.; Bulu, I.; Khan, M.; Maletinsky, P.; Yacoby, A.; Loncar, M. Enhanced single-photon emission from a diamond-silver aperture. *Nat. Phot.* **2011**, 5, 738-743.
- 18 Hennessy, K.; Badolato, A.; Winger, M.; Gerace, D.; Atature, M.; Guide, S.; Faelt, S.; Hu, E. L.; Imamoglu, A. Quantum nature of a strongly coupled single quantum dot-cavity system. *Nature* **2007**, 445, 896-899.
- 19 Bulu, I.; Babinec, T.; Hausmann, B.; Choy, J. T.; Loncar, M. Plasmonic resonators for enhanced diamond NV-center single photon sources. *Opt. Expr.* **2011**, 19, 5268-5276.
- 20 Wenger, J.; Gerard, D.; Dintinger, J.; Mahboub, O.; Bonod, N.; Popov, E.; Ebbesen, T. W.; Rigneault, H. Emission and excitation contributions to enhanced single molecule fluorescence by gold nanometric apertures. *Opt. Expr.* **2008**, 16, 3008-3020.
- 21 Aouani, H.; Mahboub, O.; Bonod, N.; Devaux, E.; Popov, E.; Rigneault, H.; Ebbesen, T. W.; Wenger, J. Bright unidirectional fluorescence emission of molecules in a nanoaperture with plasmonic corrugations. *Nano Lett.* **2011**, 11, 637-644.

- 22 Pibiri, E.; Holzmeister, P.; Lalkens, B.; Acuna, G. P.; Tinnefeld, P. Single-molecule positioning in zeromode waveguides by DNA origami nanoadapters. *Nano Lett.* **2014**, 14, 3499-3503.
- 23 Aouani, H.; Iltzhakov, S.; Gachet, D.; Devaux, E.; Ebbesen, T. W.; Rigneault, H.; Oron, D.; Wenger, J. Colloidal quantum dots as probes of excitation field enhancement in photonic antennas. *ACS Nano* **2010**, 4, 4571-4578.
- 24 Jun, Y. C.; Huang, K. C. Y.; Brongersma, M. L. Plasmonic beaming and active control over fluorescent emission. *Nat. Comms.* **2011**, 2, 283.
- 25 Wang, C. F.; Badolato, A.; Wilson-Rae, I.; Petroff, P. M.; Hu, E.; Urayama, J.; Imamoglu, A. Optical properties of single InAs quantum dots in close proximity to surfaces. *Appl. Phys. Lett.* **2004**, 85, 3423-3425.
- 26 Andersen, M. L.; Stobbe, S.; Sorensen, A. S.; Lodahl, P. Strongly modified plasmon-matter interaction with mesoscopic quantum emitters. *Nat. Phys.* **2011**, 7, 215-218.
- 27 Kurtsiefer, C.; Mayer, S.; Zarda, P.; Weinfurter, H. Stable solid-state source of single photons. *Phys. Rev. Lett.* **2000**, 85, 290-293.
- 28 Majumdar, A.; Bajcsy, M.; Rundquist, A.; Vuckovic, J. Loss-enabled sub-poissonian light generation in a bimodal nanocavity. *Phys. Rev. Lett.* **2012**, 108, 183601.
- 29 Jelezko, F.; Wrachtrup, J. Single defect centres in diamond: A review. *Phys. stat. sol. (a)* **2006**, 203, 3207-3225.
- 30 Castelletto, S.; Johnson, B. C.; Ivady, V.; Stagrias, N.; Umeda, T.; Gali, A.; Oshima, T. A silicon carbide room-temperature single photon source. *Nat. Mat.* **2014**, 13, 151-156.
- 31 Palik, E. D. In *Handbook of optical constants of solids III*; Academic Press: San Diego, 1998; Ch. 7.
- 32 Landau, L. D.; Lifshitz, E. M.; Pitaevskii, L. P. In *Electrodynamics of continuous media*; Pergamon: London, 1976, p. 275.